

An automated end-to-end deep learning-based framework for lung cancer diagnosis by detecting and classifying the lung nodules

Samiul Based Shuvo

Department of Biomedical Engineering

Bangladesh University of Engineering and Technology, Dhaka 1205, Bangladesh

E-mail: sbshuvo@bme.buet.ac.bd

Abstract — Objective: Lung cancer is a leading cause of cancer-related deaths worldwide, and early detection is crucial for improving patient outcomes. Nevertheless its early diagnosis cancer is a major challenge, particularly in low resource settings where access to medical resources and trained radiologists is limited. The objective of this study is to propose an automated end-to-end deep learning-based framework for the early detection and classification of lung nodules, specifically for low-resource settings. Methods: The proposed framework consists of three stages: lung segmentation using modified 3D U-Net named 3D Res-U-Net, nodule detection using YOLO-v5, and classification with a Vision Transformer-based architecture. We evaluated the proposed framework on a publicly available dataset, LUNA16. The proposed framework's performance was measured using the respective domain's evaluation matrices. Results: The proposed framework achieved 98.82% lung segmentation dice score while detecting the lung nodule with 0.76 mAP@50 from the segmented lung, at a low false-positive rate. The performance of both networks of the proposed framework were compared with other studies and found to outperform them regarding segmentation and detection accuracy. Additionally, our proposed Vision transformer network obtained an accuracy of 93.57%, which is 1.21% higher than the state-of-the-art networks. Conclusion: Our proposed end-to-end deep learning-based framework can effectively segment lung, and detect and classify lung nodules, specifically in low-resource settings with limited access to radiologists. The proposed framework outperforms existing studies regarding all the respective evaluation metrics. Significance: The proposed framework can potentially improve the accuracy and efficiency of lung cancer screening in low-resource settings, ultimately leading to better patient outcomes. Our study demonstrates that deep learning-based approaches can be effectively applied to automated lung cancer detection and classification, even in settings with limited medical resources and trained personnel.

Index Terms— Deep Learning, Lung Segmentation, Lung Nodule, Lung Cancer, U-Net, Vision Transformer, YOLO-V5

I. INTRODUCTION

Lung cancer has the greatest fatality rate (18%) and the second-highest incidence rate (11.4%) among all malignant tumors worldwide, according to statistics from the GLOBOCAN 2020 cancer report [1]. In poor or underdeveloped nations, lung cancer cases account for more than half of all cases [?]. Just 15% of lung cancer patients survive five years after diagnosis, and 70% have either locally progressed or distant metastases [2]. The major cause of this is that individuals with early-stage lung cancer frequently don't show any symptoms, which causes a delayed diagnosis and worse results. Pulmonary nodules are the main symptom of early-stage lung cancer, and early identification of lung cancer is essential to increasing survival rates [3], [4]. Accurately identifying lung nodules with a diameter between 3mm and 30mm is essential for early diagnosis and lowering death rates.

Doctors use computed tomography (CT) imaging to locate pulmonary nodules and spot early-stage lung cancer. However, because they lack sufficient medical equipment and supplies, developing nations find it difficult to access this technology. Additionally, because

CT exams are time-consuming, challenging, and require radiologists to examine hundreds of images, the likelihood that a misdiagnosis will be made increases. However, the automatic diagnosis of pulmonary nodules has some issues, such as the vast difference between the number of positive and negative samples, the different shapes of the nodules, and the lack of integrated approaches [4], [5]. Computer-aided diagnosis (CAD) can help with these problems by making doctors' jobs easier, making diagnosis faster, and reducing the number of incorrect diagnoses.

In this study, we present an integrated end-to-end Cascaded Tri-Stage Framework (CTSF) for automatically locating pulmonary nodules and determining whether or not they are malignant. The CTSF comprises three phases that identify and categorize pulmonary nodules. A 2D-based Yolov5 network is utilized to detect lung nodules on axial slices after the lung is segmented using a novel 3D Res-Unet-based lung segmentation network. By this, the region of interest (ROI) is detected. The third and last level is a 2D classification network that extracts nodule characteristics and forecasts their diagnostic score using a self-attention-based, vision transformer with the patch of the slice extracted according to the detection network's predicted ROI. A flow diagram of the proposed CTSF is shown in Fig. 1.

The contributions of this paper are as follows:

- We establish the CTSF using multi-stage models. Our framework can reliably and properly identify and categorize pulmonary nodules from top to bottom, reducing the burden on clinicians and the rate of incorrect diagnoses.
- We propose a novel 3D Res-Unet algorithm, which can segment the lung with State of the art performance.
- We utilize the Yolo-V5 detection algorithm, which can detect the lung nodule with high confidence performance.
- We utilize a novel vision transformer-based classification network that classifies the cancerous nodule.
- Our proposed approach obtains 89.5% dice lung segmentation score and 89% lung nodule detection mAP on the LUNA16 dataset [6] and 86.75% cancer classification accuracy.

The remainder of this paper is organized as follows. Section II reviews related work in the field of lung cancer detection and highlights the strengths and limitations of existing approaches. Section III presents utilized datasets and their preprocessing schemes. In Section IV, we introduce the design of the CTSF in detail, including three architectures employed, and the evaluation metrics used to assess the framework's performance. Section VI presents the experimental results and VII discusses the strengths and limitations of our proposed approach. Finally, Section VIII summarizes the contributions of this work and outlines directions for future research.

II. RELATED WORKS

As mentioned, several studies explored segmenting the lung parenchyma, identifying nodules, and categorizing malignant nodules utilizing ML and DL-based frameworks using publicly and privately

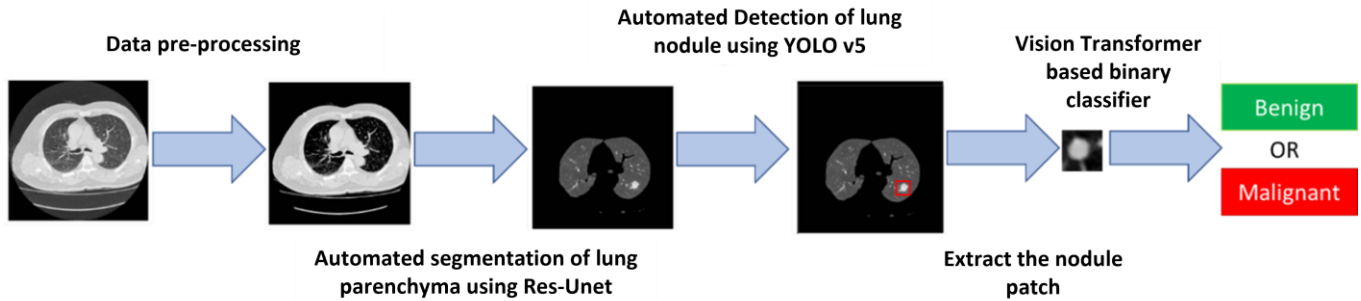


Fig. 1. A graphical overview of the end-to-end deep learning-based framework for lung cancer detection workflow.

TABLE I

SUMMARY OF WORKS CARRIED OUT IN SEGMENTATION, NODULE DETECTION AND CLASSIFICATION DOMAIN ON LUNG CT .

Lung Segmentation Task			
Author	Dataset	Network	Dice Score(%)
Badrinarayanan et al. [7] (2017)	LUNA16	Segnet	96.52
Alom et al. [8] (2019)	LUNA16	R2U-Net	98.80
Khanna et al. [9] (2020)	LUNA16	ResNet 34 based U-Net	96.57
Jalali et al. [10] (2021)	LIDC-IDRI	BCDU-Net	97.31
Francis et al. [11] (2022)	AAPM Lung CT Segmentation Challenge 2017 dataset	3D U-Net	Left lung: 97.9 Right Lung: 97.3
Lung Nodule Detection Task			
Author	Dataset	Network	mAP@50
Cai et al. [12] (2020)	LUNA16	Mask R-CNN	0.88
Shao et al. [13] 2021	LUNA16	Yolo v5 refined	0.75
Zhou et al. [14] (2022)	LUNA16	Yolo v5(s)	0.75
Liu et al. [15] (2022)	LUNA16	STBi-YOLO	0.95
Lung Nodule Malignancy Classification Task			
Author	Dataset	Network	Accuracy(%)
de Carvalho Filho et al. [16] (2018)	LIDC-IDRI	CNN	92.63
Xie et al. [17] (2018)	LIDC-IDRI	DCNN	89.53
Huang et al. [18] (2022)	LIDC-IDRI	SSTL-DA	91.07
Wu et al. [19] (2023)	LIDC-IDRI	STLF-VA	92.36

accessible datasets. In this part, we offered an overview of research activities in this domain (shown in Table I).

III. MATERIALS AND METHODS

In this section, an overview of the used datasets, signal pre-processing stages are provided.

A. Datasets

1) *Lung Nodule Analysis(LUNA16) Dataset* : The Lung Nodule Analysis(LUNA16) Dataset comprises a set of CT scans that focus on detecting pulmonary nodules in the chest CT scan. The dataset was created to facilitate the development of automated nodule detection systems for clinical use, as part of the 2016 International Symposium on Biomedical Imaging (ISBI) Lung Nodule Analysis (LUNA) Challenge. It consists of CT scans from 888 patients, with a total of 1,186 nodules annotated by four experienced radiologists. To ensure accuracy, a two-phase annotation process was used, and nodules larger than 3mm were considered by all four radiologists [6]. It also includes lung segmentation binary mask for each CT scan. This dataset is widely recognized as a benchmark for nodule detection research and has been extensively used for training deep learning models and comparing the performance of different nodule detection algorithms.

B. Data preprocessing

Lung CT scans typically display the whole chest cavity, however, pulmonary nodules are only visible in the left and right lobes. Sometimes, spherical tissues resembling nodules near the lobes may impede accurate identification. The raw CT data must be preprocessed and the lung parenchyma extracted to overcome this obstacle. This method decreases the detection area and increases the accuracy of future diagnoses.

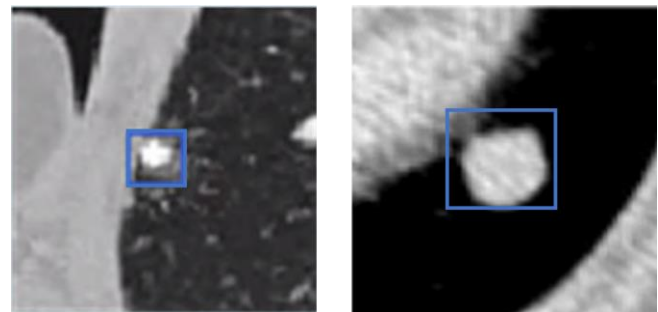


Fig. 2. Some instances of nodules very near the lung surface.

TABLE II
DETAILS OF HYPERPARAMETERS USED FOR THE MODELS.

Lung Segmentation Task		Lung Nodule Detection Task		Lung Nodule Malignancy Classification Task	
Hyper-parameters	Values	Hyper-parameters	Values	Hyper-parameters	Values
Training data	800	Training data	6045	Training data	1577
Test data	88	Test data	756	Test data	394
Batch size	4	Batch size	64	Batch size	256
Learning rate	0.0001	Learning rate	0.01	Learning rate	0.0001
Epoch	60	Epoch	600	Epoch	60
Optimizer	Adam	Optimizer	Adam	Optimizer	Adam
Loss function	Dice loss	Loss function	Box loss — bounding box regression loss Obj loss — the objectness loss Cls loss — the classification loss	Loss function	Categorical-cross entropy
				Patch Size	8

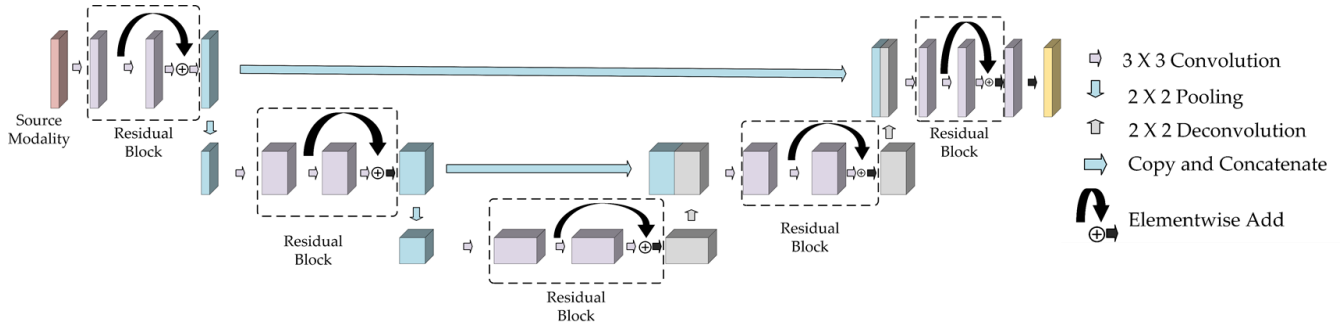


Fig. 3. Overview of the proposed 3D Res-UNet architecture.

C. Detection Network

The Hounsfield (HU) unit is used to represent CT data in a simple and standardized manner, however HU values may vary across tissues. By altering the HU value range, the detecting area may be controlled.

The stages involved in data preparation are as follows:

- **Data normalization:** The HU value range of lung parenchyma is $[-1200, 600]$, thus we normalize the picture HU value range to this range [20].
- **Mapping:** The HU value range is mapped to $[0, 1]$ using Min-Max normalization.
- **Binarization of Mask:** The given ground truth mask has many settings, including 1 for the backdrop and 3 or 4 for the left and right lungs. We assign 0 to the backdrop and 1 to both lung regions.
- **Respacing and Resizing of Picture and Mask:** We resized the data to $256 \times 256 \times 256$ and resized it to 1mm in the x, y, and z dimensions.

To prepare data for YOLO-V5, the following steps need to be taken:

- **Crop foreground:** Crop the empty space around the segmented lung parenchyma based on the largest foreground size.
- **Generate bounding box:** Use the spherical mask to generate a bounding box for each slice based on the provided diameter and center in the annotation file. The YOLO-V5 label format should include the class ID, x-center, y-center, width, and height with normalized box coordinates.

To train the classification network, we cropped a 64×64 slice from the spherical mask volume based on the annotation file's diameter and center.

IV. DEEP LEARNING ARCHITECTURES

A. Segmentation Network

Lung CT scans often reveal the patient's complete chest cavity. Several spherical tissues next to the lobe appeared like nodules.

Thus, it is required to analyze the raw CT data and remove the lung parenchyma. On the other hand, different types of nodules are occurring in the lung. Some of them are extremely near to the lung surface (see Fig. 2).

Thus maintaining a dependable and more accurate segmentation network is essential. That is why we are adopting 3D methods that appear significantly better in the lung segmentation task,

1) **Baseline Model-3D Unet**: Comparable to the standard Unet [21], our 3D Unet model has an analysis and synthesis route with four resolution stages (Number of filters 24, 48, 96, 192, consecutively) in each. Each layer in the analysis route consists of two $3 \times 3 \times 3$ convolutions, a rectified linear unit (ReLU), and a $2 \times 2 \times 2$ max pooling with two strides in each dimension. In the synthesis route, each layer consists of a $2 \times 2 \times 2$ up convolution with two strides in each dimension, followed by two $3 \times 3 \times 3$ convolutions, each followed by a ReLU. To supply the synthesis route with the necessary high-resolution characteristics, short-cut connections from layers of equivalent resolution in the analysis path are used. In the last layer, a $1 \times 1 \times 1$ convolution lowers the output channels to the number of labels, in this instance 3, using a $1 \times 1 \times 1$ convolution. The input to the network is an image tile of $256 \times 256 \times 256$ voxels, and the output in the last layer is $256 \times 256 \times 1$ voxels in the x, y, and z directions, respectively.

2) **Proposed Model(3D Res-UNet)**: The most crucial element of a deep residual network is the residual block, which comprises of convolutional layers with identity mapping, as seen in the figure 3. The residual block is intended to reduce the gradient vanishing problem, and it may also improve the information transmission between layers. In this study, four subunits (four convolutional layers in the Residual block) were used.

YOLOv5 is a state-of-the-art deep learning model for object detection that uses a single neural network to predict object bounding boxes and class probabilities in an input image. The model is an improvement over its predecessors, YOLOv4 and YOLOv3, and uses several new techniques to achieve high accuracy and efficiency. The YOLOv5 model consists of a CSPNet (Cross-Stage Partial Network) backbone, which is a more efficient variant of the Darknet backbone

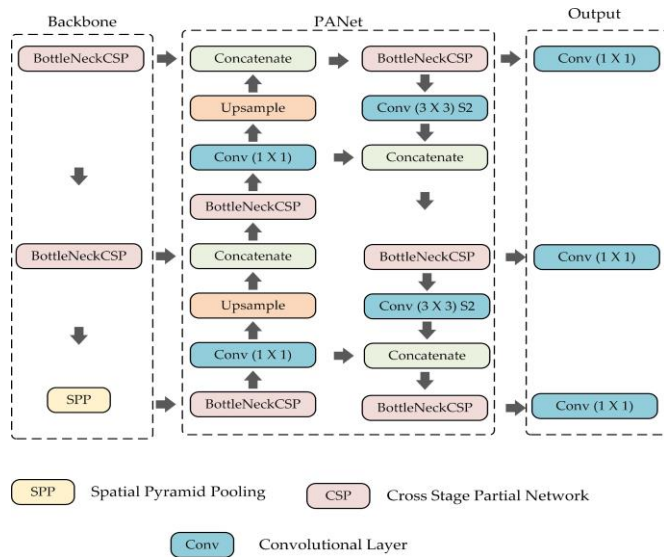


Fig. 4. The main parts of the YOLOv5 model are the CSPDarknet backbone, the PANet neck, and the YOLO Layer head. In the CSPDarknet, features are extracted from the data, and in the PANet, the features that were extracted are combined. The final object detection results, including class, score, location, and size, are generated by the YOLO layer.

used in previous versions of YOLO. The CSPNet backbone is used to extract features from the input image, which are then passed through several layers of spatial pyramid pooling (SPP) and path aggregation network (PAN) modules to improve the model's ability to capture features at different scales (are shown in 4).

The YOLOv5 model uses anchor boxes to predict object bounding boxes, and a novel loss function called the GIoU (Generalized Intersection over Union) loss to train the model. The GIoU loss is a modification of the traditional Intersection over Union (IoU) loss, and provides a better measure of the similarity between predicted and ground truth bounding boxes. In addition, the YOLOv5 model uses a technique called self-ensemble, where multiple versions of the same model are used to make predictions on the same input image. The predictions from the different models are then combined to produce a final prediction, which has been shown to improve the model's accuracy [22]. The YOLOv5 model comes in several different variants, ranging from YOLOv5s (small) to YOLOv5x (extra large). The larger models have more parameters and are able to achieve higher accuracy, but are also more computationally expensive to train and run. In this study we have the small version of this model due to computation constraint.

B. Classification Network

Vision Transformer (ViT) is a deep learning architecture for computer vision applications that Google researchers introduced in 2020 [23]. Unlike traditional convolutional neural networks (CNNs), ViT employs self-attention processes from the transformer architecture to extract global context from pictures. Our proposed ViT network first breaks down the input nodule patches into 8 smaller patches. Then it executes a series of linear transformations on these patches to convert them into a sequence of tokens. These tokens are delivered into 8 successive transformer encoders, which apply multi-head self-attention with a projection dimension of 64 and feed-forward layers with 64 and 128 hidden nodes to learn features of the image. Eventually, a feed-forward network with sequential 2048 and

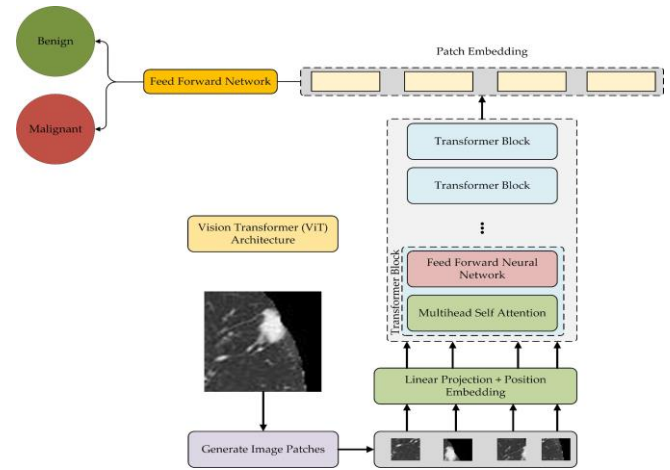


Fig. 5. Overview of the proposed vision transformer architecture.

1024 hidden states helps learn from the retrieved characteristics that assist the final classification layer anticipate the output label.

V. EXPERIMENTAL EVALUATION

A. Experimental setup

The deep learning architectures are implemented using Pytorch, TensorFlow and Keras, while all the models are trained and tested on Intel(R) Xeon(R) CPU and NVidia GTX 2080 Ti GPU. which were trained on 4 RTX A4500 with a total 80 GB GPU with 24 GB VRAM and an Intel Core i9-10920X CPU with 12 cores with a clock speed of 3.50 GHz with 256 GB RAM.

10% of the training data was kept for validation during the training of all the models. Additionally, in classification model training, a mini-batch balancing scheme is employed to pass an equal number of samples from each class on all the batches.

B. Evaluation metrics for lung segmentation

The Dice score is a commonly used metric for evaluating the performance of a lung segmentation algorithm by measuring the pixel-wise agreement between the predicted lung segmentation and its corresponding ground truth. The Dice score is calculated as follows:

$$\text{Dice score} = \frac{2 \times |X \cap Y|}{|X| + |Y|} \quad (1)$$

In this formula, X and Y represent two sets, and $|X|$ and $|Y|$ represent their respective cardinalities (i.e., the number of elements in each set). The symbol \cap represents the intersection of the two sets (i.e., the set of elements that are common to both X and Y), and $|X \cap Y|$ represents the cardinality of their intersection. The Dice score is a measure of similarity between two sets, with a value ranging from 0 (no similarity) to 1 (perfect similarity)

C. Evaluation metrics for lung nodule detection

For evaluate the performance of the YOLO-v5 nodule detection network two $mAP@50$ and $mAP@50:95$ have been utilized. $mAP@50$ is the mean average precision at a detection threshold of 50% for the official PASCAL VOC (Visual Object Classes) dataset. It is calculated as follows:

$$mAP@50 = \frac{1}{N_{classes}} \sum_{i=1}^{N_{classes}} AP_{50}^i \quad (2)$$

where $N_{classes}$ is the number of object classes, and AP_{50}^i is the average precision for class i at a detection threshold of 50%.

mAP@50:95 is the mean average precision averaged over all recall values between 50% and 95% for the official COCO (Common Objects in Context) dataset. It is calculated as follows:

$$mAP@50 : 95 = \frac{1}{N_{classes}} \sum_{i=1}^{N_{classes}} \int_{0.5}^{0.95} AP(r) dr \quad (3)$$

where $N_{classes}$ is the number of object classes, $AP(r)$ is the average precision at recall level r , and the integral is taken over all recall levels from 50% to 95%.

D. Evaluation metrics for cancer classification

The cancer classification LC-ViT framework is evaluated quantitatively using well-known and important performance evaluation metrics such as Accuracy, Precision, Recall, and F1-score. The formulas for these metrics are as follows:

Accuracy(Acc.) measures the proportion of correctly classified samples, and is calculated as:

$$Acc. = \frac{TP + TN}{TP + FP + TN + FN} \quad (4)$$

Precision measures the proportion of positive samples that are correctly identified, and is calculated as:

$$Precision = \frac{TP}{TP + FP} \quad (5)$$

Recall measures the proportion of positive samples that are correctly identified out of all the positive samples, and is calculated as:

$$Recall = \frac{TP}{TP + FN} \quad (6)$$

F1-score combines both precision and recall into a single metric, and is calculated as the harmonic mean of precision and recall:

$$F1 \text{ score} = \frac{2 * TP}{2 * TP + FP + FN} \quad (7)$$

where TP, TN, FP, and FN represent the number of true positives, true negatives, false positives, and false negatives, respectively.

VI. EXPERIMENTAL RESULTS

A. Segmentation results

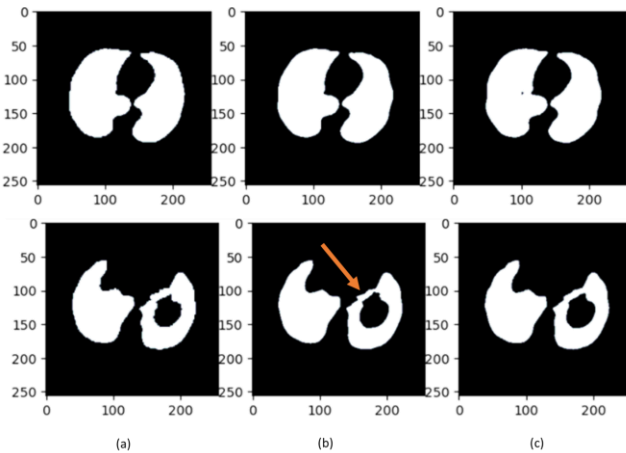


Fig. 6. The visual results of lung segmentation for 3D U-Net and 3D Res-U-Net architecture. (a), (b) and (c) column represents Ground truth, 3D U-Net prediction, and 3D Res-U-Net prediction.

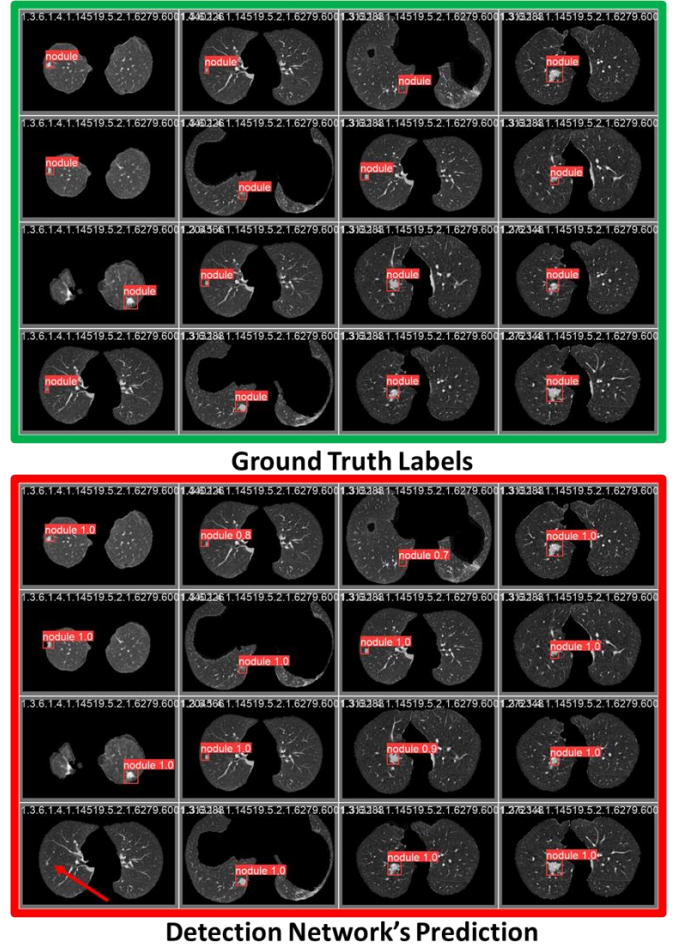


Fig. 7. Detection results of nodules on LUNA16 dataset using YOLOv5(s).

TABLE III

COMPARISON OF THE PROPOSED FRAMEWORK WITH EXISTING LUNG SEGMENTATION METHODS.

Author	Network	Dice Score(%)	F1-Score (%)
Badrinarayanan et al. [7]	SegNet	96.52	95.75
Alom et al. [8]	R2U-Net	98.80	98.79
Khanna et al. [9]	ResNet 34 based U-Net	98.63	-
Jalali et al. [10]	Res-BCDU-Net	97.31	98.05
Our [1]	3D U-Net	97.97	97.94
	3D Res-U-Net	98.82	98.73

We compared the results of our lung segmentation to the expert-provided ground truth lung masks in order to evaluate the effectiveness of the suggested segmentation process. To quantify the comparison, we employed two distinct metrics: Dice score (DSC) and F1-score. In order to examine the impact of residual connections, we used two distinct models to assess the performance of the suggested approach: 3D-U-Net and 3D-Res-U-Net, a modified version of 3D-U-Net. Table III displays the overall performance of different architectures. We used 3D-U-Net and 3D-Res-U-Net to get average DSC and F1 scores of 97.54 and 97.54 for the LUNA dataset, respectively. The 3D-Res-U-Net model denotes the suggested method's capacity to generalize to samples that haven't been seen before.

Additionally, the 3D-Res-U-Net performed noticeably better than any previous cutting-edge lung segmentation networks. To ensure that there is neither an overfitting nor an underfitting phenomenon, we also examined the learning curve of the suggested approach for lung CT

TABLE IV
COMPARISON OF THE PROPOSED FRAMEWORK WITH
EXISTING NODULE DETECTION METHODS.

Author	Network	mAP@50	mAP@50:95
Cai et al. [12]	Mask R-CNN	0.88	0.571
Shao et al. [13]	Yolo v5 refined	0.75	-
Zhou et al. [14]	Yolo v5(s)	0.75	-
Liu et al. [15]	STBi-YOLO	0.95	-
Our Proposed	YOLOv5(s)	0.76	0.62

segmentation in terms of dice loss.

We also examined the suggested method's visual outcomes, and Figure 6 demonstrates that there was little to no mistake in creating the segmentation mask of the lung area from the input lung CT images. The 3D-Res-U-Net effectively handled the most difficult region of the lung due to its higher performance, but 3D-U-Net was unable to recreate the most complicated curvatures (as seen by the red arrow in Fig. 6).

B. Nodule detection results

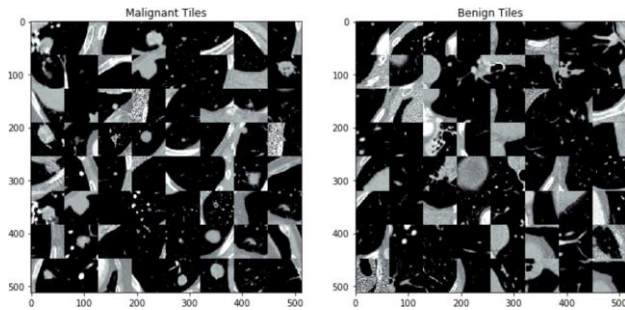


Fig. 8. Representation of some malignant and benign nodules

We evaluated YOLOv5(s) with other common nodule detection strategies with recent publications to confirm its efficacy in single-stage lung nodule identification. Table IV displays the comparison's findings between our model, YOLO-v5, YOLO-v5s, and Mask R-CNN. Comparing the YOLO-v5s to the one-stage SSD and the two-stage Mask R-CNN, it can be said that the YOLO-v5s is a more compact network model. The YOLO-v5 model we used consistently performed to other cutting-edge architectures. However, STBi-YOLO showed significantly better performance compared to all other models. We noticed that the preprocessing techniques and training data preparation process have not been well-mentioned in [15].

We also examined the suggested method's visual outcomes, and Fig. 7 demonstrates that there was little to no mistake in detecting the the lung nodule from the segmented lung CT input images. The YOLOv5 handled the most difficult nodule, but sometimes less-represented classes or small nodules are missed by the detection algorithm.(as seen by the (See red arrow in Fig. 7).

C. Cancer classification results

We evaluated our proposed Vision Transformer algorithm on LUNA16 datasets, and we collected diagnostic information from the LIDC-IDRI lung nodule datasets [24], which are the main sets of the LUNA16 dataset. Examples of binary class nodules are shown in Fig. 8, and Table V compares our suggested model's

TABLE V
COMPARISON OF THE PROPOSED FRAMEWORK WITH
EXISTING NODULE'S MALIGNANCY CLASSIFICATION
METHODS.

Author	Network	Acc.(%)	Recall(%)	Precision(%)
de Carvalho Filho et al. [16]	CNN	92.03	93.47	90.70
Xie et al. [17]	DCNN	89.93	92.02	84.19
Huang et al. [18]	SSTL-DA	91.07	91.22	90.93
Wu et al. [19]	STLF-VA	92.36	93.08	90.93
Our Proposed	ViT	93.57	93.10	90.95

performance metrics with state-of-the-art (SOTA) methods. All the articles mentioned utilized the LIDC-IDRI database. It is clear from the table that our ViT model shows promising performance compared to existing works. For example, authors in Wu et al. used STLF-VA classifiers and reported accuracies of 92.36%. Our model obtained an accuracy and precision of 93.57% and 90.95%, respectively, which is 1.21% and 0.02% higher than the previously top-performing method [19].

VII. LIMITATIONS & FUTURE WORKS

Although the proposed framework showed promising results, it requires a significant amount of computational resources such as powerful GPUs and large amounts of memory. This may limit its practicality in low-resource settings. Additionally, the system has not been validated in clinical settings and further studies are needed to assess its effectiveness in assisting clinicians in making primary decisions for lung cancer diagnosis. [25], [26]

In the future, we plan to test the framework on larger and more diverse datasets including in-house one to ensure its applicability. Additionally, we aim to incorporate this framework into clinical decision support systems to aid radiologists in making accurate diagnoses and treatment plans. However, since deep neural networks are often seen as black boxes, we also plan to use gradient-weighted class activation mapping (GradCAM) to maintain the model's interpretability while retaining its complexity [27].

VIII. CONCLUSIONS

In this study, we proposed a complete end-to-end automatic deep neural framework for the classification of benign and malignant lung nodules, which enables the detection of cancer from input CT scans. Our proposed framework leverages three consecutive architectures, namely 3D-Res-UNet, YOLO-V5, and ViT architectures, to achieve this task. The experimental results demonstrate that the proposed framework can reliably segment the lung, detect the nodules, and classify the pathological condition of those nodules with high accuracy. Notably, our ViT architecture achieved an overall accuracy of 93.57%, outperforming other state-of-the-art architectures. We believe that our proposed system can be utilized to automatically classify lung cancer and assist in making primary decisions in real-world clinical scenarios, particularly in third-world countries.

IX. COMPLIANCE WITH ETHICAL STANDARDS

Author contributions All the works performed by Samiul Based Shuvo.

Funding None.

Conflict of interest Author certifies that he has no affiliations with or involvement in any organization or entity with any financial interest or non-financial interest in the subject matter or materials

discussed in this manuscript.

Ethical approval This article does not contain any studies on human participants or animals performed by the author.

Research involving human participants and/or animals This article does not contain any studies with human participants or animals performed by the author.

Informed consent This article does not contain any studies on human participants performed by the author.

REFERENCES

- [1] H. Sung, J. Ferlay, R. L. Siegel, M. Laversanne, I. Soerjomataram, A. Jemal, and F. Bray, "Global cancer statistics 2020: Globocan estimates of incidence and mortality worldwide for 36 cancers in 185 countries," *CA: a cancer journal for clinicians*, vol. 71, no. 3, pp. 209–249, 2021.
- [2] M. B. Amin, "American joint committee on cancer, american cancer society," p. 1024, 2017.
- [3] H. Chen, W. Xiong, J. Wu, Q. Zhuang, and G. Yu, "Decision-making model based on ensemble method in auxiliary medical system for non-small cell lung cancer," *IEEE Access*, vol. 8, pp. 171 903–171 911, 2020.
- [4] J. Wu, Y. Tan, Z. Chen, and M. Zhao, "Decision based on big data research for non-small cell lung cancer in medical artificial system in developing country," *Computer Methods and Programs in Biomedicine*, vol. 159, pp. 87–101, 2018.
- [5] A. Shrivastava, A. Gupta, and R. Girshick, "Training region-based object detectors with online hard example mining," in *Proceedings of the IEEE conference on computer vision and pattern recognition*, 2016, pp. 761–769.
- [6] A. A. A. Setio, A. Traverso, T. De Bel, M. S. Berens, C. Van Den Bogaard, P. Cerello, H. Chen, Q. Dou, M. E. Fantacci, B. Geurts *et al.*, "Validation, comparison, and combination of algorithms for automatic detection of pulmonary nodules in computed tomography images: the luna16 challenge," *Medical image analysis*, vol. 42, pp. 1–13, 2017.
- [7] V. Badrinarayanan, A. Kendall, and R. Cipolla, "Segnet: A deep convolutional encoder-decoder architecture for image segmentation," *IEEE transactions on pattern analysis and machine intelligence*, vol. 39, no. 12, pp. 2481–2495, 2017.
- [8] M. Z. Alom, C. Yakopcic, M. Hasan, T. M. Taha, and V. K. Asari, "Recurrent residual u-net for medical image segmentation," *Journal of Medical Imaging*, vol. 6, no. 1, pp. 014 006–014 006, 2019.
- [9] A. Khanna, N. D. Londhe, S. Gupta, and A. Semwal, "A deep residual u-net convolutional neural network for automated lung segmentation in computed tomography images," *Biocybernetics and Biomedical Engineering*, vol. 40, no. 3, pp. 1314–1327, 2020.
- [10] Y. Jalali, M. Fateh, M. Rezvani, V. Abolghasemi, and M. H. Anisi, "Resbcdu-net: a deep learning framework for lung ct image segmentation," *Sensors*, vol. 21, no. 1, p. 268, 2021.
- [11] S. Francis, P. Jayaraj, P. Pournami, M. Thomas, A. T. Jose, A. J. Binu, and N. Puzhakkal, "Thoraxnet: a 3d u-net based two-stage framework for oar segmentation on thoracic ct images," *Physical and Engineering Sciences in Medicine*, vol. 45, no. 1, pp. 189–203, 2022.
- [12] L. Cai, T. Long, Y. Dai, and Y. Huang, "Mask r-cnn-based detection and segmentation for pulmonary nodule 3d visualization diagnosis," *Ieee Access*, vol. 8, pp. 44 400–44 409, 2020.
- [13] Z. Shao, G. Wang, and C. Zhou, "Imageological examination of pulmonary nodule detection," in *2021 2nd International Conference on Big Data & Artificial Intelligence & Software Engineering (ICBASE)*. IEEE, 2021, pp. 383–386.
- [14] Z. Zhou, F. Gou, Y. Tan, and J. Wu, "A cascaded multi-stage framework for automatic detection and segmentation of pulmonary nodules in developing countries," *IEEE Journal of Biomedical and Health Informatics*, vol. 26, no. 11, pp. 5619–5630, 2022.
- [15] K. Liu, "Stbi-yolo: A real-time object detection method for lung nodule recognition," *IEEE Access*, vol. 10, pp. 75 385–75 394, 2022.
- [16] A. O. de Carvalho Filho, A. C. Silva, A. C. de Paiva, R. A. Nunes, and M. Gattass, "Classification of patterns of benignity and malignancy based on ct using topology-based phylogenetic diversity index and convolutional neural network," *Pattern Recognition*, vol. 81, pp. 200–212, 2018.
- [17] Y. Xie, J. Zhang, Y. Xia, M. Fulham, and Y. Zhang, "Fusing texture, shape and deep model-learned information at decision level for automated classification of lung nodules on chest ct," *Information Fusion*, vol. 42, pp. 102–110, 2018.
- [18] H. Huang, R. Wu, Y. Li, and C. Peng, "Self-supervised transfer learning based on domain adaptation for benign-malignant lung nodule classification on thoracic ct," *IEEE Journal of Biomedical and Health Informatics*, vol. 26, no. 8, pp. 3860–3871, 2022.
- [19] R. Wu, C. Liang, Y. Li, X. Shi, J. Zhang, and H. Huang, "Self-supervised transfer learning framework driven by visual attention for benign-malignant lung nodule classification on chest ct," *Expert Systems with Applications*, vol. 215, p. 119339, 2023.
- [20] W. Tan and H. Guo, "Data augmentation and cnn classification for automatic covid-19 diagnosis from ct-scan images on small dataset," in *2021 20th IEEE International Conference on Machine Learning and Applications (ICMLA)*. IEEE, 2021, pp. 1455–1460.
- [21] O. Ronneberger, P. Fischer, and T. Brox, "U-net: Convolutional networks for biomedical image segmentation," in *Medical Image Computing and Computer-Assisted Intervention—MICCAI 2015: 18th International Conference, Munich, Germany, October 5-9, 2015, Proceedings, Part III 18*. Springer, 2015, pp. 234–241.
- [22] G. Jocher, A. Chaurasia, A. Stoken, J. Borovec, NanoCode012, Y. Kwon, K. Michael, TaoXie, J. Fang, imyhxy, Lorna, Yifu), C. Wong, A. V. D. Montes, Z. Wang, C. Fati, J. Nadar, Laughing, and M. Jain, "ultralytics/yolov5: v7.0 - YOLOv5 SOTA Realtime Instance Segmentation (v7.0)," 2022. [Online]. Available: <https://doi.org/10.5281/zenodo.7347926>
- [23] A. Dosovitskiy, L. Beyer, A. Kolesnikov, D. Weissenborn, X. Zhai, T. Unterthiner, M. Dehghani, M. Minderer, G. Heigold, S. Gelly *et al.*, "An image is worth 16x16 words: Transformers for image recognition at scale," *arXiv preprint arXiv:2010.11929*, 2020.
- [24] S. G. Armato III, G. McLennan, L. Bidaut, M. F. McNitt-Gray, C. R. Meyer, A. P. Reeves, B. Zhao, D. R. Aberle, C. I. Henschke, E. A. Hoffman *et al.*, "The lung image database consortium (lidc) and image database resource initiative (idri): a completed reference database of lung nodules on ct scans," *Medical physics*, vol. 38, no. 2, pp. 915–931, 2011.
- [25] J. Acharya and A. Basu, "Deep neural network for respiratory sound classification in wearable devices enabled by patient specific model tuning," *IEEE transactions on biomedical circuits and systems*, vol. 14, no. 3, pp. 535–544, 2020.
- [26] S. Y. Nikouei, Y. Chen, S. Song, R. Xu, B.-Y. Choi, and T. R. Faughnan, "Real-time human detection as an edge service enabled by a lightweight cnn," in *2018 IEEE International Conference on Edge Computing (EDGE)*. IEEE, 2018, pp. 125–129.
- [27] H. W. Loh, C. P. Ooi, S. Seoni, P. D. Barua, F. Molinari, and U. R. Acharya, "Application of explainable artificial intelligence for healthcare: A systematic review of the last decade (2011–2022)," *Computer Methods and Programs in Biomedicine*, vol. 226, p. 107161, 2022. [Online]. Available: <https://www.sciencedirect.com/science/article/pii/S0169260722005429>